Reprinted from
Journal of Imaging Science and Technology® 60(6): 060405-1–060405-8, 2016.
https://doi.org/10.2352/ISSN.2470-1173.2017.12.IQSP-218

Blind Image Quality Assessment Using Multiscale Local Binary Patterns

Pedro Garcia Freitas
Department of Computer Science, University of Brasília, Brasília, Brazil

Welington Y. L. Akamine
Department of Electrical Engineering, University of Brasília, Brasília, Brazil

Mylène C. Q. Farias▲
Department of Computer Science, University of Brasília, Brasília, Brazil
Department of Electrical Engineering, University of Brasília, Brasília, Brazil
E-mail: mylene@ieee.org

Abstract. *This article proposes a new no-reference image quality assessment method that is able to blindly predict the quality of an image. The method is based on a machine learning technique that uses texture descriptors. In the proposed method, texture features are computed by decomposing images into texture information using multiscale local binary pattern (MLBP) operators. In particular, the parameters of local binary pattern operators are varied, which generates MLBP operators. The features used for training the prediction algorithm are the histograms of these MLBP channels. The results show that, when compared with other state-of-the-art no-reference methods, the proposed method is competitive in terms of prediction precision and computational complexity.* © *2016 Society for Imaging Science and Technology.*

INTRODUCTION

Given the high volume of visual media available, the task of assessing the visual quality of a content is becoming increasingly important. In particular, image quality assessment (IQA) methods are often necessary to estimate the performance of compression techniques,[1] transmission processes, displays, enhancement and restoration algorithms,[2] or any type of image processing technique.

There are two types of IQA methods: subjective and objective.[3] Subjective quality assessment methods consist of psychophysical experiments in which human subjects estimate the quality of a series of stimuli.[4] These experiments are expensive, laborious, time-consuming, and, therefore, hard to incorporate into an automatic system. On the other hand, in objective quality assessment methods, computer algorithms substitute psychophysical experiments, making it possible to implement fast and cheap procedures for monitoring and controlling the quality of images.[5]

Objective image quality assessment methods are generally classified into three classes, according to the amount of reference information required by the algorithm.[6] If the full reference (original image) is required to estimate the image quality, the algorithm is classified as a full-reference (FR) method. When only partial information about the reference (e.g., features extracted from the original image) is used, the algorithm is classified as a reduced-reference (RR) method. Since requiring even partial reference information is an impediment for several multimedia applications, in most cases the most suitable solution is to use no-reference (NR) methods, which blindly estimate the quality of a test image without requiring any information about its reference.

Although a lot of work has been carried out in the area of IQA, most efforts have been in the development of FR methods, and there are still many open questions in the area of no-reference image quality assessment (NR-IQA).[7] The development of fast and accurate NR-IQA methods is still a challenging problem, with two popular approaches. The first approach is distortion-specific NR-IQA (DS-NR-IQA), which estimates the perceived quality of an image using specific distortion measures.[8–10] The second approach is non-distortion-specific NR-IQA (NDS-NR-IQA). NDS-NR-IQA methods are generally based on the assumption that natural images cover a small subset of all possible images (including distorted images), and, therefore, a statistical comparison between test images and the subset of natural images can be used to obtain a quality estimate.[11–13]

NDS-NR-IQA methods that perform a statistical comparison between impaired and non-impaired natural images are known as "natural scene statistic" (NSS)-based methods. As mentioned earlier, NSS methods are based on an analysis of the statistical regularities of non-distorted natural images, considering a set of features or artifacts. For example, Saad et al.[13] have successfully used Discrete Cosine Transform (DCT) domain statistics to determine the model parameters that are sensitive to most commonly perceived artifacts. Sheikh et al.[14] have developed an NR-IQA method using

▲ IS&T Member.

Received July 3, 2016; accepted for publication Oct. 21, 2016; published online Dec. 7, 2016. Associate Editor: Yeong-Ho Ha.

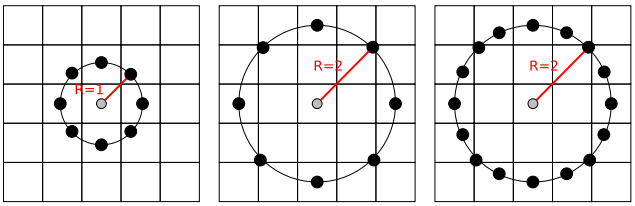

(a) $R = 1, P = 8$ (b) $R = 2, P = 8$ (c) $R = 2, P = 16$

Figure 1. Circularly symmetric P neighbors extracted from a distance R.

joint histograms of adjacent wavelet coefficients. More recently, Liu et al.[15] proposed an NR-IQA method that uses a set of statistical features extracted from the curvelet representation of an image.

Another way to develop NDS-NR-IQA methods is to use machine learning (ML) techniques to identify patterns that characterize different quality levels. While NSS-based approaches analyze the statistical differences between impaired and non-impaired images for specific artifacts, ML approaches delegate to the computer the task of recognizing which patterns better reflect the changes in quality caused by the presence of artifacts. Given the complex non-linear processes that underlie human perception and contribute to quality perception, we believe that the use of machine learning and pattern recognition techniques can lead to NR-IQA methods with good accuracy performance. Among the several NDS-NR-IQA methods that use machine learning, we can mention the works of Ye et al.,[16,17] Zhang et al.,[18,19] Liu et al.,[20] and Freitas et al.[21] Although these ML methods show promising results, they have limitations, especially in terms of computational complexity and prediction performance.

To overcome the above-mentioned limitations, we propose a new ML NDS-NR-IQA method. Instead of making assumptions about specific image artifacts or statistical differences between impaired and non-impaired images, the proposed method uses pattern recognition techniques to analyze texture information and predict image quality. To the best of our knowledge, the only other methods that have used a similar approach were proposed by Ye et al.[16] and Freitas et al.[21] Ye et al.[16] used large codebooks of complex and computationally expensive Gabor-filter-based features to perform an analysis of the image textures. To estimate quality, their algorithm compares distorted and non-distorted image patches. Freitas et al.[21] used an extension of the local binary pattern (LBP) descriptor, known as local ternary pattern (LTP), which uses three levels to quantize the differences between a pixel and its neighbor. The method is fast and reliable, but it produces poor results for some specific artifacts.

The method proposed in this article has the goal of investigating the influence of a multiscale operator on the sensitivity to image impairments and, therefore, improving the accuracy performance. Instead of using LTP operators like Freitas et al.,[21] in this work we use fast texture feature extractors, which are multiscale versions of the local binary pattern (LBP) operators. More specifically, the multiscale

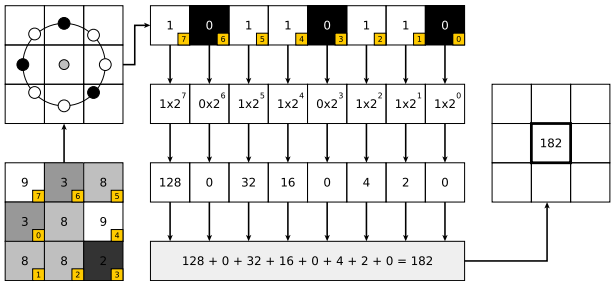

Figure 2. Calculation of LBP labels.

LBP (MLBP) operator applies the regular LBP operator for multiple radius and sampling point parameters. The MLBP operator was proposed by Ojala et al.[22] and has been used in several applications, such as face recognition[23] and texture analysis.[24] In this article, we adapt the MLBP operators to efficiently capture the texture properties that are affected by quality changes. We use a set of public image databases to measure the prediction accuracy and computational time of the proposed method. When compared with current state-of-the-art NR-IQA methods, the proposed method has a lower computational complexity and a higher quality prediction accuracy.

LOCAL BINARY PATTERN OPERATOR

The local binary pattern (LBP) is arguably one of the most powerful texture descriptors. It was first proposed by Ojala et al.,[25,26] and has since been proven to be an effective feature extractor for texture-based problems. The traditional LBP operator[22] takes the form

$$LBP_{R,P}(I_c) = \sum_{p=0}^{P-1} S(I_p - I_c)2^p, \tag{1}$$

where

$$S(t) = \begin{cases} 1, & t \geq 0, \\ 0, & \text{otherwise.} \end{cases} \tag{2}$$

In Eq. (1), $I_c = I(x, y)$ is an arbitrary central pixel at the position (x, y) and $I_p = I(x_p, y_p)$ is a neighboring pixel surrounding I_c, where $x_p = x + R\cos\left(2\pi(p/P)\right)$ and $y_p = y - R\sin\left(2\pi(p/P)\right)$. P is the total number of neighboring pixels I_p, sampled with a distance R from I_c. Figure 1 illustrates examples of symmetric samplings with different numbers of neighboring points (P) and radius (R) values.

Figure 2 illustrates the steps for applying the LBP operator on a single pixel ($I_c = 8$) located in the center of a 3×3 image block, as shown in the bottom left of this figure. The numbers in the yellow squares of the block represent the order in which the operator is computed (counter-clockwise direction starting from 0). In this figure, we use a unitary neighborhood radius ($R = 1$) and eight neighboring pixels ($P = 8$). After calculating $S(t)$ (Eq. (2)) for each neighboring pixel I_p, we obtain a binary output for each I_p ($0 \leq p \leq 7$), as illustrated in the block in the upper-left position of Fig. 2.

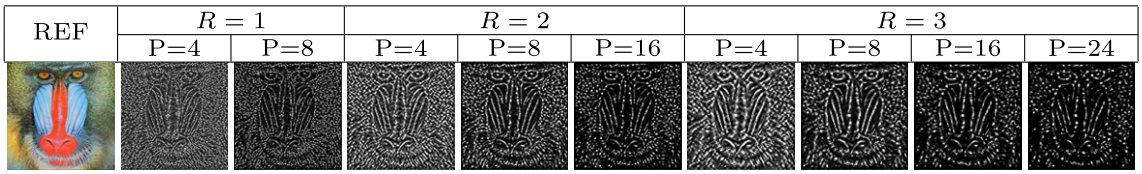

Figure 3. Reference image and its corresponding local binary pattern (LBP) channels computed using three different radius (R) values.

In this block, black circles correspond to "0" and white circles to "1." These binary outputs are stored in a binary format, according to their position (yellow squares). Then, the resulting binary number is converted to the decimal format. This decimal number is the output generated by the LBP operator for I_c. After applying the operator for all pixels in an image, we obtain a set of labels, which is known as the *LBP channel*. Figure 3 shows examples of LBP channels for the image "Baboon," obtained using different radius values and numbers of neighboring points.

When an image is rotated, the I_p sampled values move along the perimeter of the circumference around I_c, generating a circular shift in the binary number generated. As a consequence, a different decimal $LBP_{R,P}(I_c)$ value is obtained. To remove this effect, we can use the following rotation-invariant operator:

$$LBP^{ri}_{R,P}(I_c) = \min\{ROTR(LBP_{R,P}(I_c), k)\}, \qquad (3)$$

where $k = \{0, 1, 2, \cdots, P-1\}$ and $ROTR(x, k)$ is the circular bit-wise right shift operator that shifts the tuple x by k positions.

Due to the crude quantization of the angular space and the occurrence of specific frequencies in individual patterns,[26,27] $LBP_{R,P}$ and $LBP^{ri}_{R,P}$ operators do not always provide a good discrimination.[27] To improve the discriminability, Ojala et al.[22] proposed an improved operator that captures fundamental pattern properties. These fundamental patterns are called "uniform" and are computed as follows:

$$LBP^{u}_{R,P}(I_c) = \begin{cases} \sum_{p=0}^{P-1} S(I_p - I_c), & U(LBP^{ri}_{R,P}) \leq 2, \\ P+1, & \text{otherwise}, \end{cases} \qquad (4)$$

where $U(LBP_{P,R}) = \Delta(I_{P-1}, I_0) + \sum_{p=1}^{P-1} \Delta(I_p, I_{p-1})$, and $\Delta(I_x, I_y) = |S(I_x - I_c) - S(I_y - I_c)|$. In addition to a better discriminability, the uniform LBP operator described in Eq. (4) has the advantage of generating fewer distinct LBP labels. While the "non-uniform" operator (Eq. (1)) produces 2^P different output values, the uniform operator produces only $P+2$ distinct output values.

IMAGE QUALITY ASSESSMENT METHOD

The proposed method is based on the assumption that visual impairments alter image textures and their statistics. In other words, images with similar impairments, at similar strengths, have textures that share similar statistical properties. Therefore, features extracted by the proposed method are basically statistics of texture descriptors that capture changes in quality. The proposed algorithm has two main stages: (1) feature extraction and (2) image quality prediction.

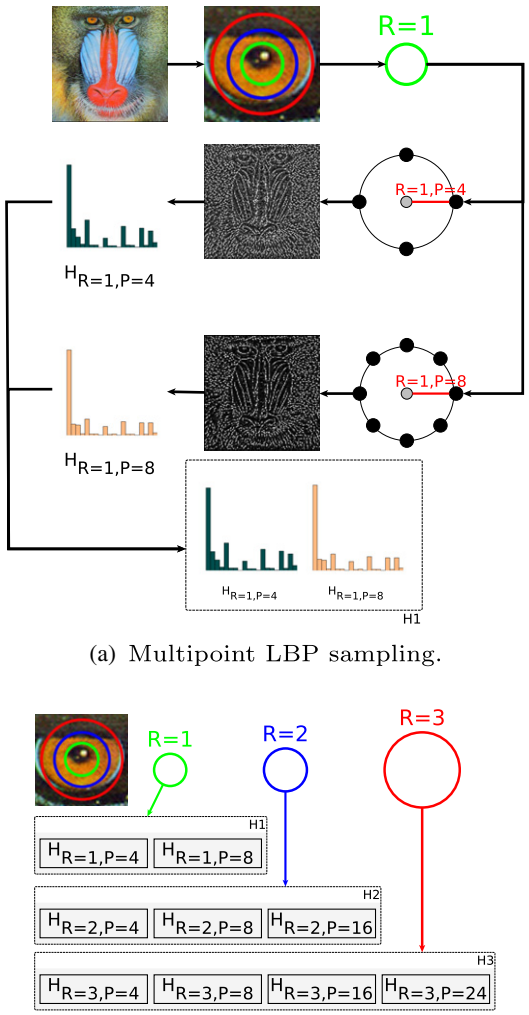

(a) Multipoint LBP sampling.

(b) Multiple histogram generation from LBP.

Figure 4. Feature extraction steps.

An illustration of the feature extraction stage is depicted in Figure 4. Using the methods described in the previous section, we compute several LBP channels by varying the parameters R and P and performing a symmetrical sampling. For the smallest possible radius, $R = 1$, there are two possible P values that produce rotational symmetrical sampling ($P = 4$ and $P = 8$). When $R = 2$, there are three possible P values ($P = 4$, $P = 8$, and $P = 16$). In general, for a given radius R, there are a total of $R + 1$ distinct LBP channels.

Fig. 4(a) depicts the feature extraction for $R = 1$. The unitary radius generates only two distinct symmetrical

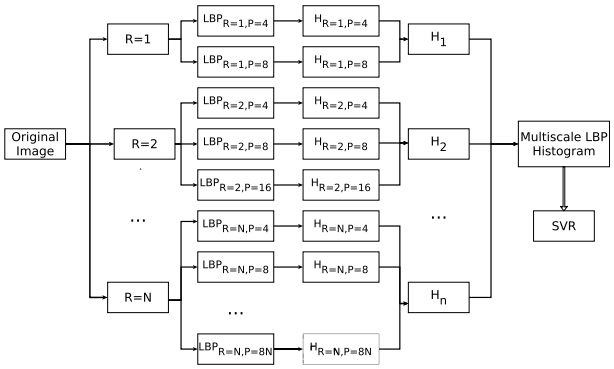

Figure 5. Feature extraction using multiscale LBP histograms.

patterns ($P = 4$ and $P = 8$). Each pattern generates a distinct LBP channel (see Fig. 3). From these LBP channels, a texture feature is obtained by computing the histogram of the operator outputs. For a radius R, LBP maps are generated:

$$L_R = \{LBP^u_{R,4}, LBP^u_{R,8}, LBP^u_{R,16}, \ldots, LBP^u_{R,8R}\}, \quad (5)$$

where $LBP^u_{R,P}$ is computed according to Eq. (4) and L_R contains $R + 1$ elements. Then, the histogram of each member of L_R is created:

$$H_{R,P} = \left[h_{R,P}(l_1), h_{R,P}(l_2), \cdots, h_{R,P}(l_{P+2})\right], \quad (6)$$

where

$$h_{R,P}(l_i) = \sum_{x,y} \delta(LBP^u_{R,P}(x, y)i), \quad (7)$$

and

$$\delta(s, t) = \begin{cases} 1, & s = t, \\ 0, & \text{otherwise.} \end{cases} \quad (8)$$

In the above equations, (x, y) indicates the position of a given point of $LBP^u_{R,P}$ and l_i is the ith LBP label. Notice that we are using uniform LBP operators (Eq. (4)) since their histograms provide a better discrimination of the texture properties.

To obtain the feature vector, we vary the radius, and compute all possible symmetric LBP patterns and their histograms. This process is illustrated in Fig. 4(b). For a radius R, we generate a vector of histograms by concatenating all individual LBP histograms:

$$H_R = H_{R,4} \oplus H_{R,8} \oplus H_{R,16} \oplus \cdots \oplus H_{R,8R}, \quad (9)$$

where $\oplus$ denotes the concatenation operator.

The steps for computing the multiscale LBP histogram are summarized in Figure 5. For $R = N$, the final feature vector is generated by concatenating the histograms of the LBP channels with radius values smaller than N:

$$x = x_N = H_1 \oplus H_2 \oplus H_3 \oplus \cdots \oplus H_N, \quad (10)$$

where $R = N$ is the maximum radius value and x_N is the feature vector used to compute the histogram.

The feature vector x, composed of the concatenated histograms, is used as input to the support vector regression (SVR) algorithm. Since we compute the histogram of all LBP operators with radius values less than or equal to N to obtain x, we name this operator *multiscale LBP* (MLBP). A support vector regression algorithm is used to predict the image quality from the feature vector x. The SVR has been shown to be a very robust algorithm for high-dimensional feature spaces.[28] To train the quality model with SVR, the feature vectors are mapped to subjective quality scores in a training stage:

$$Q_{predicted}(I) = SVR(x, \Omega), \quad (11)$$

where Ω is the trained model and $Q_{predicted}(I)$ is the objective quality score predicted using the model.

EXPERIMENTAL SECTION

The proposed algorithm was compared with the fastest state-of-the-art NR-IQA methods. The chosen algorithms are BRISQUE,[29] CORNIA,[17] CQA,[15] SSEQ,[30] and LTP.[21] Additionally, we also compared the proposed algorithm with two well-established FR-IQA metrics, namely PSNR and SSIM.[31] The performance of the methods was measured using three established correlation coefficients: Spearman's rank ordered correlation (SROCC), Pearson (linear) correlation coefficient (LCC), and Kendall's rank correlation coefficient (KRCC). The correlation coefficients are computed between the scores predicted using the IQA methods and the corresponding subjective scores are provided in the video quality databases. The databases used in this work are as follows.

- CSIQ:[32] This database has a total of 866 test images, consisting of 30 originals and six different categories of distortions.
- LIVE2:[33] This database has 982 test images, including 29 originals and five categories of distortions. The distortions include JPEG, JPEG 2000 (JPEG2k), white noise (WN), Gaussian blur (GB), fast fading (FF), global contrast decrements (CD), and additive Gaussian pink noise (PN).
- TID2013:[34] This database contains 25 reference images with the following distortions: additive Gaussian noise (AGN), additive noise in color components (AGC), spatially correlated noise (SCN), masked noise (MN), high frequency noise (HFN), impulse noise (IN), quantization noise (QN), Gaussian blur (GB), image denoising (ID), JPEG, JPEG2k, JPEG transmission errors (JPEGTE), JPEG2k transmission errors (JPEG2kTE), non-eccentricity pattern noise (NEPN), local block-wise distortions (LBD), intensity shift (IS), contrast change (CC), change of color saturation (CCS), multiplicative Gaussian noise (MGN), comfort noise (CN), lossy compression (LC), image color quantization with dither (ICQ), chromatic aberration (CA), and sparse sampling and reconstruction (SSR).

Since all chosen NR methods are SVR-based methods, all simulations were performed following the same procedure. After the feature extraction stage of each method, the SVR algorithm is used to map the features into the

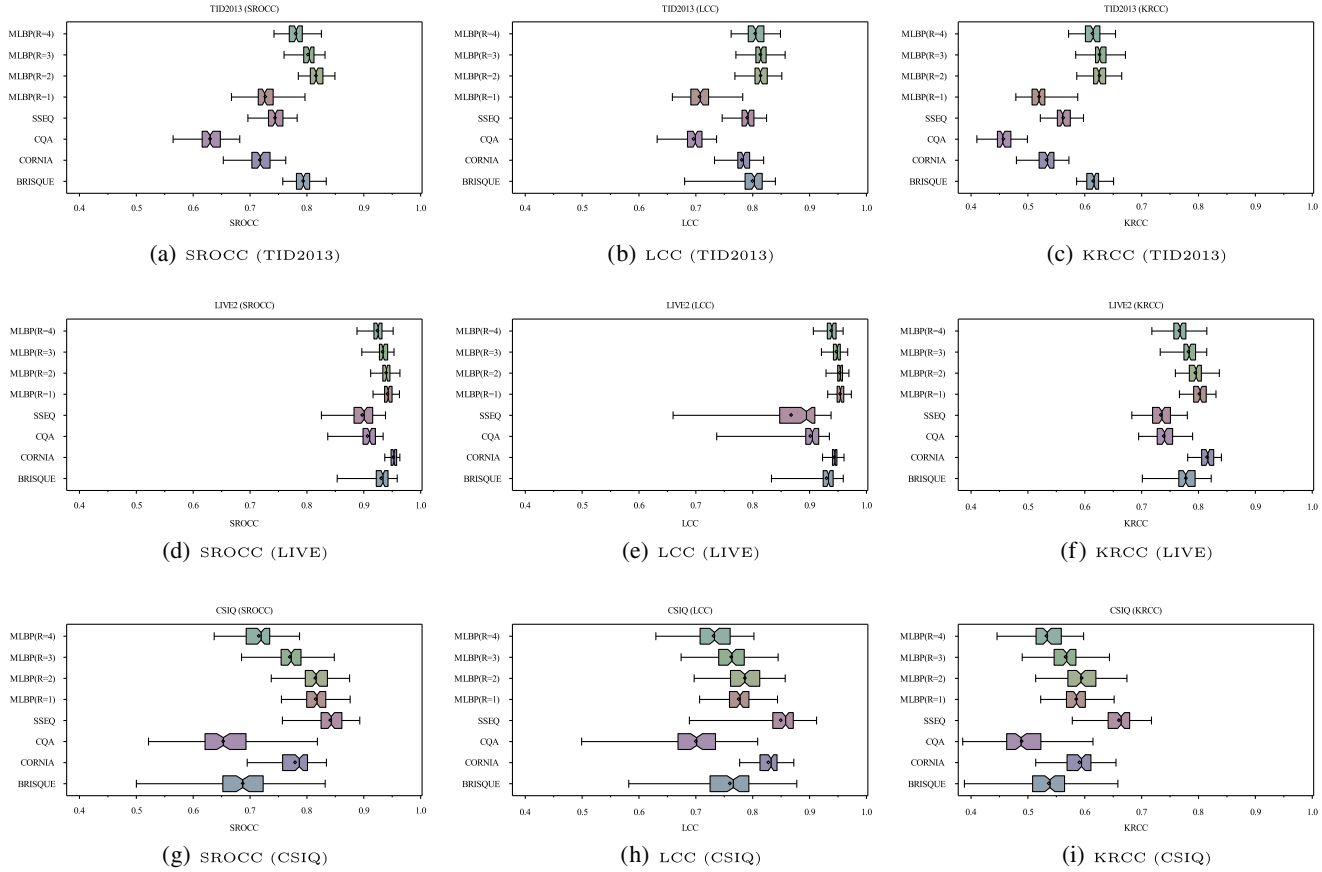

(a) SROCC (TID2013) (b) LCC (TID2013) (c) KRCC (TID2013)

(d) SROCC (LIVE) (e) LCC (LIVE) (f) KRCC (LIVE)

(g) SROCC (CSIQ) (h) LCC (CSIQ) (i) KRCC (CSIQ)

Figure 6. Box plot of SROCC, LCC, and KRCC distributions of NR algorithms from 100 runs of simulations using the TID2013 (a–c), LIVE (d–f), and CSIQ (g–i) databases.

subjective scores provided in the video quality databases. We use an SVR implementation provided by LibSVM, which has a Python interface supported by the Scikit library.[35] To perform the simulations and obtain the best performance for all methods, we use ν-SVR with a radial basis function (RBF) kernel. The optimal metaparameters (C, γ, ν, etc.) are automatically found using exhaustive grid search methods provided by Sklearn's API.

To train the machine learning NR-IQA methods, the databases are split into training and testing subsets. For each simulation, the subsets are randomly selected, with 80% of data used for training and 20% for testing. The reported results correspond to the median values obtained for 100 simulations with random combinations of training and testing subsets. Figure 6 depicts the box plots of the correlation coefficients for all tested NR-IQA methods. In this figure, the proposed method is indicated as "MLBP," followed by the radius R used as parameter.

From Fig. 6, we notice that the proposed method presents a higher performance in the TID2013 database for all cases where $R > 1$. The SROCC values (Fig. 6(a)) reveal that the proposed method presents better performance when $R = 2$, but the LCC and KRCC values indicate that a better performance is achieved when $R = 3$. For the LIVE database (Fig. 6(d)–(f)), we can notice that the proposed method outperforms most of the tested NR-IQA methods. Nevertheless, the proposed method and CORNIA present similar performance. It is worth pointing out that CORNIA is the most computationally expensive method tested in our work, as depicted in Table II. Interestingly, the unitary radius ($R = 1$) provides the best performance in the LIVE database, which is different from the results obtained for the TID2013 database. For the CSIQ database, the performance of the proposed method is (statistically) similar to the performance of CORNIA. Considering SROCC (Fig. 6(g)), the proposed method (for $R \in \{1, 2, 3\}$) outperforms all methods with the exception of SSEQ. In terms of LCC (Fig. 6(h)), the proposed method performs worse than CORNIA and SSEQ. However, when KRCC (Fig. 6(i)) is considered, the results of the proposed method are similar to the results of CORNIA.

Although Fig. 6 allows a visual comparison of tested methods, it does not show the individual performance of the metrics for each database. Table I presents the LCC values obtained for the sets of images containing each distortion type. In this table, the numbers in italics represent the best median correlation for a given distortion type, considering both NR and FR methods. The numbers in bold correspond to the best median correlation among the NR-IQA methods. We can notice that PSNR produces the best correlation values for the TID2013 and CSIQ databases. However, the proposed method outperforms many of the tested NR-IQA methods.

Table I. Median SROCC of simulations using the TID2013, LIVE, and CSIQ databases.

									LBP				σ	
		PSNR	SSIM	BRISQUE	CORNIA	CQA	SSEQ	LTP	$R=1$	$R=2$	$R=3$	$R=4$	σ_{all}	σ_{prop}
TID2013	AGC	0.8568	0.7912	***0.9289***	0.7362	0.9192	0.9269	0.7523	0.6196	0.7934	0.8320	0.8189	0.0937	0.0989
	AGN	*0.9337*	0.6421	0.8559	0.4046	0.6436	0.8321	0.8623	0.7367	0.8626	***0.9067***	0.8958	0.1599	0.0781
	CA	0.7759	0.7158	0.8460	0.7450	0.6504	0.7665	0.8739	0.8314	***0.9042***	0.8764	0.8114	0.0772	0.0422
	CC	*0.4608*	0.3477	0.0143	0.1992	**0.3093**	0.0204	0.1196	0.1604	0.1619	0.1834	0.2068	0.1335	0.0218
	CCS	0.6892	0.7641	0.1265	0.1781	0.1562	0.3098	0.7223	0.4019	0.5691	0.6525	***0.8958***	0.2733	0.2056
	CN	*0.8838*	0.6465	0.6357	0.7577	0.1025	0.3211	**0.7685**	0.5396	0.7462	0.7206	0.7238	0.2263	0.0960
	GB	0.8905	0.8196	0.8844	0.9008	0.9169	0.8715	***0.9423***	0.8035	0.8938	0.8307	0.7405	0.0586	0.0636
	HFN	0.9165	0.7962	0.8689	0.8531	0.9238	***0.9270***	0.9	0.8263	0.8684	0.8963	0.9076	0.0422	0.0362
	ICQ	*0.9087*	0.7271	0.8436	0.7931	0.8196	**0.9008**	0.8743	0.7678	0.7594	0.7534	0.7421	0.0653	0.0108
	ID	*0.9457*	0.8327	0.8854	0.7665	0.8403	0.8438	0.8726	0.8625	0.9053	**0.9062**	0.8823	0.0473	0.0209
	IN	*0.9263*	0.8055	0.8663	0.6962	0.6531	0.8310	**0.8962**	0.6356	0.7380	0.7038	0.6997	0.1010	0.0427
	IS	*0.7647*	0.7410	**0.4497**	0.0896	0.1396	0.3704	0.3158	0.3096	0.3678	0.3529	0.2942	0.2104	0.0349
	JPEG	*0.9252*	0.8275	0.8145	0.8467	0.7805	0.8315	**0.8877**	0.7185	0.8291	0.8123	0.7573	0.0570	0.0508
	JPEGTE	0.7874	0.6144	0.6709	0.7450	0.3842	0.5096	0.8138	0.4856	0.8011	0.8070	***0.8154***	0.1553	0.1612
	JPEG2k	0.8934	0.7531	***0.9119***	0.8788	0.8881	0.8819	0.9015	0.8623	0.8822	0.8584	0.8075	0.0464	0.0318
	JPEG2kTE	*0.8581*	0.7067	0.6151	**0.7085**	0.6496	0.6878	0.6815	0.5099	0.6082	0.6223	0.6513	0.0858	0.0613
	LBD	0.1300	0.6213	0.6915	0.2258	0.3250	0.5343	***0.6969***	0.5780	0.6689	0.6560	0.6546	0.2024	0.0414
	LC	*0.9386*	0.8310	**0.9144**	0.8269	0.5691	0.7019	0.8607	0.6624	0.8100	0.8278	0.8281	0.1101	0.0802
	MGN	0.9085	0.7863	***0.9287***	0.6692	0.8870	0.7938	0.9202	0.7196	0.9041	0.8881	0.8879	0.0885	0.0872
	MN	*0.8385*	0.7388	**0.8332**	0.4846	0.6858	0.7807	0.7928	0.4553	0.6299	0.6121	0.5990	0.1331	0.0802
	NEPN	*0.6930*	0.5326	0.4708	0.3893	0.0777	0.0700	0.075	0.2143	0.4627	0.5317	**0.5747**	0.2246	0.1611
	QN	0.8636	0.7428	0.7945	0.6550	0.6777	**0.8867**	0.8223	0.7442	0.7372	0.7196	0.7034	0.0745	0.0183
	SCN	*0.9152*	0.7934	0.8634	0.9231	0.8722	0.8704	**0.9054**	0.8467	0.8845	0.8698	0.9017	0.0364	0.0233
	SSR	0.9241	0.7774	***0.9487***	0.7657	0.8403	0.9158	0.9015	0.6889	0.8436	0.8436	0.8814	0.0785	0.0855
	ALL	0.6869	0.5758	0.7939	0.7181	0.6296	0.7441	***0.8408***	0.7272	0.8164	0.8022	0.7809	0.0819	0.0391
LIVE	JPEG	0.8515	0.9480	0.9026	0.9240	0.8867	0.8848	0.9422	0.9478	**0.9484**	0.9469	0.9469	0.0341	0.0007
	JPEG2K	0.8822	0.9438	0.9109	0.9326	0.8967	0.9086	0.9418	***0.9672***	0.9569	0.9513	0.9451	0.0271	0.0094
	WN	0.9856	0.9793	0.9734	0.9672	0.9823	0.9616	0.9435	0.9885	0.9886	0.9891	***0.9892***	0.0146	0.0003
	GB	0.7818	0.8889	0.9618	***0.9738***	0.9131	0.9362	0.9423	0.9565	0.9492	0.9252	0.8925	0.0534	0.0289
	FF	0.8869	0.9335	0.8830	0.9335	0.8704	0.8527	***0.942***	0.9124	0.9337	0.9316	0.9206	0.0306	0.0099
	ALL	0.8013	0.8902	0.9336	0.9530	0.9102	0.9006	0.942	***0.9541***	0.9537	0.9477	0.9385	0.0454	0.0073
CSIQ	JPEG	0.9009	*0.9309*	0.7121	0.8743	0.6316	0.8756	**0.917**	0.8725	0.8953	0.8667	0.8263	0.0921	0.0287
	JPEG2K	*0.9309*	0.9251	0.7738	0.9033	0.8274	0.8667	**0.9172**	0.8507	0.8310	0.7590	0.6925	0.0769	0.0722
	WN	*0.9345*	0.8760	0.6425	0.8381	0.6547	**0.9164**	0.8319	0.7284	0.6597	0.6519	0.6237	0.1208	0.0444
	GB	*0.9358*	0.9089	0.6021	**0.9150**	0.6180	0.8972	0.9017	0.8922	0.8749	0.7954	0.7269	0.1219	0.0763
	PN	*0.9315*	0.8870	0.7746	0.6687	0.7319	0.8253	0.8063	0.7636	0.8539	0.8567	**0.8670**	0.0758	0.0481
	CD	*0.8862*	0.8128	0.5080	0.6131	0.5114	**0.7031**	0.0539	0.3515	0.4019	0.4383	0.4658	0.2305	0.0494
	ALL	0.8088	0.8116	0.6877	0.7865	0.6529	0.8428	***0.8636***	0.8157	0.8158	0.7698	0.7160	0.0665	0.0475

For the LIVE database, the proposed method outperforms the tested methods for almost all distortion types.

Table I also exhibits the standard deviation values of correlation values of each row. The symbol σ_{all} corresponds to the standard deviation calculated for all methods, while σ_{prop} corresponds to the standard deviation only for the proposed method. These differences give a measure of the sensitivity of the methods for different distortions. Higher values of σ_{all} indicate that distinct methods have a higher difference of prediction efficiency. From these values, we can observe that the methods are more sensitive to AGN, CC, CCS, CN, IS, JPEGTE, LBD, LC, MN, NEPN, and CD distortions. Notice that, for most cases, the proposed method presents smaller standard deviation values.

The higher the values of σ_{prop} are, the higher the impact of the parameter R is on the prediction accuracy of the proposed method. These values allow us to evaluate the distortions where more LBP channels are necessary to obtain a better prediction of the subjective scores. The higher values indicate the cases where the proposed method outperforms the other methods significantly (i.e., CCS, JPEGTE, and NEPN distortions). Furthermore, we can notice that the higher the radius is, the higher the correlation value is. This indicates that additional texture information is necessary to improve the performance of NR-IQA algorithms.

Table II shows the computational complexity of the tested NR-IQA methods. Notice that the proposed method has a low computational complexity, being considerably faster than other NR-IQA algorithms. The average computational time (measured over all test images in the three tested databases) is around 0.08 seconds per image for $R=1$. For the tests, we used a PC with an Intel i7-4790 processor at 3.60 GHz. This result makes the proposed method very competitive for real-time applications.

DISCUSSION

Although the proposed method outperforms other state-of-the-art methods, its performance can be further improved by incorporating additional pattern recognition techniques, like, for example, a distortion classification algorithm.[36] Since quality prediction performance may vary as a function of the distortion type, determination of the distortion type can help in choosing the best MLBP setup.

Table II. Average computational time to perform a single objective quality assessment (in seconds).

	PSNR	SSIM	BRISQUE	CORNIA	CQA	SSEQ	LTP	LBP			
								$R=1$	$R=2$	$R=3$	$R=4$
Time	0.0055	0.0447	0.1576	1.8964	1.3691	1.8112	0.0392	0.0847	0.2688	0.8864	1.0404

Another issue that can be addressed in future work is the MLBP sensitivity to contrast change and color impairments. This is still an open question in the area of image quality,[7] and even state-of-the-art IQA methods fail to address this issue (see Table I). The proposed method exhibits a better performance when predicting the quality of images with changes in color saturation, which seem to require a set of features with higher dimensions. In future work, we plan to investigate the inclusion of specific contrast features with the goal of improving prediction accuracy.

Although a great deal of research on IQA has focused on improving prediction accuracy, little work has addressed the computational complexity. Chandler et al.[7] argue that improvement of runtime and memory performance is one of the main challenges in image quality research. The proposed method, due to the low computational complexity of the MLBP operators, requires a small memory space and a low data rate. Moreover, the proposed algorithm can be easily implemented on dedicated hardware. Furthermore, since MLBP operations are performed in each pixel independently, the proposed algorithm has great potential to be implemented in parallel for use in real-time applications.

CONCLUSIONS

In this article, we have presented a machine learning no-reference image quality assessment method, which uses a multiscale local binary pattern (MLBP) operator. The proposed method is simple and effective, and does not make assumptions about the types of image distortions. Experimental results on the LIVE database reveal that the proposed method outperforms other state-of-the-art no-reference image quality assessment methods. Results on the TID2013 and CSIQ databases show that the proposed method has an accuracy performance comparable to state-of-the-art general-purpose methods of higher computational complexity. Moreover, the performance of the proposed method is significantly better for chromatic aberration (CA) distortions, which are a challenge for most general-purpose NR-IQA methods. Future works include the investigation of the best MLBP parameters for prediction accuracy, especially considering contrast distortions (CC and CD).

ACKNOWLEDGMENTS

This work was supported by Conselho Nacional de Desenvolvimento Científico e Tecnológico (CNPq), by Coordenação de Aperfeiçoamento de Pessoal de Nível Superior (CAPES), by the Fundação de Apoio à Pesquisa do Distrito Federal (FAP-DF), and by the University of Brasília (UnB).

REFERENCES

[1] S. Wang, A. Rehman, Z. Wang, S. Ma, and W. Gao, "SSIM-inspired divisive normalization for perceptual video coding," *Image Processing (ICIP), 2011, 18th IEEE Int'l. Conf. on* (IEEE, Piscataway, NJ, 2011), pp. 1657–1660.

[2] X. Liu, D. Zhai, D. Zhao, G. Zhai, and W. Gao, "Progressive image denoising through hybrid graph Laplacian regularization: a unified framework," IEEE Trans. Image Process. **23**, 1491–1503 (2014).

[3] K. Seshadrinathan, R. Soundararajan, A. Bovik, and L. Cormack, "Study of subjective and objective quality assessment of video," IEEE Trans. Image Process. **19**, 1427–1441 (2010).

[4] M. Pinson, L. Janowski, and Z. Papir, "Video quality assessment: subjective testing of entertainment scenes," IEEE Signal Process. Mag. **32**, 101–114 (2015).

[5] S. Chikkerur, V. Sundaram, M. Reisslein, and L. Karam, "Objective video quality assessment methods: a classification, review, and performance comparison," IEEE Trans. Broadcast. **57**, 165–182 (2011).

[6] A. Ebrahimi Moghdam, P. Mohammadi, and S. Shirani, "Subjective and objective quality assessment of image: A survey," Majlesi J. Electrical Engng. **9** (2015) APA http://mjee.iaumajlesi.ac.ir/index/index.php/ee/article/view/1376/pdf_47.

[7] D. M. Chandler, "Seven challenges in image quality assessment: past, present, and future research," ISRN Signal Process. **2013** (2013).

[8] S. Wang, C. Deng, B. Zhao, G.-B. Huang, and B. Wang, "Gradient-based no-reference image blur assessment using extreme learning machine," Neurocomputing **174**, 310–321 (2016).

[9] T. Chabardès and B. Marcotegui, "Local blur estimation based on toggle mapping," *Mathematical Morphology and its Applications to Signal and Image Processing* (Springer, Reykjavik, Iceland, 2015), pp. 146–156, https://doi.org/10.1007/978-3-319-18720-4_13.

[10] L. Li, Y. Zhou, W. Lin, J. Wu, X. Zhang, and B. Chen, "No-reference quality assessment of deblocked images," Neurocomputing **177**, 572–584 (2016).

[11] A. K. Moorthy and A. C. Bovik, "Blind image quality assessment: from natural scene statistics to perceptual quality," IEEE Trans. Image Process. **20**, 3350–3364 (2011).

[12] Y. Fang, K. Ma, Z. Wang, W. Lin, Z. Fang, and G. Zhai, "No-reference quality assessment of contrast-distorted images based on natural scene statistics," IEEE Signal Process. Lett. **22**, 838–842 (2015).

[13] M. A. Saad, A. C. Bovik, and C. Charrier, "Blind image quality assessment: a natural scene statistics approach in the DCT domain," IEEE Trans. Image Process. **21**, 3339–3352 (2012).

[14] H. R. Sheikh, A. C. Bovik, and L. Cormack, "No-reference quality assessment using natural scene statistics: JPEG2000," IEEE Trans. Image Process. **14**, 1918–1927 (2005).

[15] L. Liu, H. Dong, H. Huang, and A. C. Bovik, "No-reference image quality assessment in curvelet domain," Signal Process., Image Commun. **29**, 494–505 (2014).

[16] P. Ye and D. Doermann, "No-reference image quality assessment based on visual codebook," *Image Processing (ICIP), 2011, 18th IEEE Int'l. Conf. on IEEE* (IEEE, Piscataway, NJ, 2011), pp. 3089–3092.

[17] P. Ye, J. Kumar, L. Kang, and D. Doermann, "Unsupervised feature learning framework for no-reference image quality assessment," *Computer Vision and Pattern Recognition (CVPR), 2012, IEEE Conf. on IEEE* (IEEE, Piscataway, NJ, 2012), pp. 1098–1105.

[18] M. Zhang, J. Xie, X. Zhou, and H. Fujita, "No reference image quality assessment based on local binary pattern statistics," *Visual Communications and Image Processing (VCIP), 2013, IEEE* (IEEE, Piscataway, NJ, 2013), pp. 1–6.

[19] M. Zhang, C. Muramatsu, X. Zhou, T. Hara, and H. Fujita, "Blind image quality assessment using the joint statistics of generalized local binary pattern," IEEE Signal Process., Lett. **22**, 207–210 (2015).
[20] L. Liu, Y. Hua, Q. Zhao, H. Huang, and A. C. Bovik, "Blind image quality assessment by relative gradient statistics and adaboosting neural network," Signal Process., Image Commun. **40**, 1–15 (2016).
[21] P. G. Freitas, W. Y. L. Akamine, and M. C. Q. Farias, "No-reference image quality assessment based on statistics of Local Ternary Pattern," *Eighth Int'l. Conf. on Quality of Multimedia Experience (QoMEX), 2016, IEEE* (IEEE, Piscataway, NJ, 2016), pp. 1–6.
[22] T. Ojala, M. Pietikainen, and D. Harwood, "Multiresolution gray-scale and rotation invariant texture classification with local binary patterns," IEEE Trans. Pattern Anal. Mach. Intell. **24**, 971–987 (2002).
[23] C. Chan, J. Kittler, and K. Messer, "Multi-scale local binary pattern histograms for face recognition," *Int'l. Conf. on Biometrics* (Springer, Berlin, Heidelberg, 2007), pp. 809–818.
[24] T. Maenpaa and M. Pietikainen, "Multi-scale binary patterns for texture analysis," *Scandinavian Conf. on Image Analysis* (Springer, Berlin, Heidelberg, 2003), pp. 885–892.
[25] T. Ojala, M. Pietikainen, and D. Harwood, "Performance evaluation of texture measures with classification based on Kullback discrimination of distributions," *Proc. 12th IAPR Int'l. Conf. on Pattern Recognition* (IEEE, Piscataway, NJ, 1994), Vol. 1, pp. 582–585.
[26] T. Ojala, M. Pietikäinen, and T. Mäenpää, "Gray scale and rotation invariant texture classification with local binary patterns," *Computer Vision—ECCV 2000* (Springer, Dublin, Ireland, 2000), pp. 404–420, https://doi.org/10.1007/3-540-45054-8_27.
[27] M. Pietikäinen, T. Ojala, and Z. Xu, "Rotation-invariant texture classification using feature distributions," Pattern Recognit. **33**, 43–52 (2000).
[28] A. J. Smola and B. Schölkopf, "A tutorial on support vector regression," Stat. Comput. **14**, 199–222 (2004).
[29] A. Mittal, A. K. Moorthy, and A. C. Bovik, "No-reference image quality assessment in the spatial domain," IEEE Trans. Image Process. **21**, 4695–4708 (2012).
[30] L. Liu, B. Liu, H. Huang, and A. C. Bovik, "No-reference image quality assessment based on spatial and spectral entropies," Signal Process., Image Commun. **29**, 856–863 (2014).
[31] Z. Wang, A. C. Bovik, H. R. Sheikh, and E. P. Simoncelli, "Image quality assessment: from error visibility to structural similarity," IEEE Trans. Image Process. **13**, 600–612 (2004).
[32] E. C. Larson and D. M. Chandler, "Most apparent distortion: full-reference image quality assessment and the role of strategy," J. Electron. Imaging **19**, 011006 (2010).
[33] H. R. Sheikh, M. F. Sabir, and A. C. Bovik, "A statistical evaluation of recent full reference image quality assessment algorithms," IEEE Trans. Image Process. **15**, 3440–3451 (2006).
[34] N. Ponomarenko, L. Jin, O. Ieremeiev, V. Lukin, K. Egiazarian, J. Astola, B. Vozel, K. Chehdi, M. Carli, F. Battisti, and C.-C. J. Kuo, "Image database TID2013: peculiarities, results and perspectives," Signal Process., Image Commun. **30**, 57–77 (2015).
[35] F. Pedregosa, G. Varoquaux, A. Gramfort, V. Michel, B. Thirion, O. Grisel, M. Blondel, P. Prettenhofer, R. Weiss, V. Dubourg, J. Vanderplas, A. Passos, D. Cournapeau, M. Brucher, M. Perrot, and E. Duchesnay, "Scikit-learn: machine learning in Python," J. Mach. Learn. Res. **12**, 2825–2830 (2011).
[36] H. J. Xu, "Image distortion classification towards quality assessment based on tri-training and natural scene statistics," *Applied Mechanics and Materials* (Trans Tech Publications, Pfaffikon, Switzerland, 2014), pp. 3526–3531, https://doi.org/10.4028/www.scientific.net/AMM.602-605.3526.